

Black hole accretion preferentially occurs in gas rich galaxies^{*}

F. Vito^{1,2,3,4†}, R. Maiolino^{3,4}, P. Santini⁵, M. Brusa^{1,2,6}, A. Comastri², G. Cresci⁷, D. Farrah⁸, A. Franceschini⁹, R. Gilli², G. L. Granato¹⁰, C. Gruppioni², D. Lutz⁶, F. Mannucci⁷, F. Pozzi¹, D. J. Rosario⁶, D. Scott¹¹, M. Viero¹², C. Vignali¹

¹ *Dipartimento di Fisica e Astronomia, Università degli Studi di Bologna, Via Ranzani 1, 40127 Bologna, Italy*

² *INAF – Osservatorio Astronomico di Bologna, Via Ranzani 1, 40127 Bologna, Italy*

³ *Cavendish Laboratory, University of Cambridge, 19 J. J. Thomson Avenue, Cambridge CB3 0HE, UK*

⁴ *Kavli Institute for Cosmology, University of Cambridge, Madingley Road, Cambridge CB3 0HA, UK*

⁵ *INAF – Osservatorio Astronomico di Roma, via di Frascati 33, 00040 Monte Porzio Catone, Italy*

⁶ *Max-Planck-Institut für extraterrestrische Physik (MPE), Giessenbachstrasse 1, D-85748, Garching bei München, Germany*

⁷ *INAF – Osservatorio Astrofisico di Arcetri, Largo E. Fermi 5, 50125 Firenze, Italy*

⁸ *Department of Physics, Virginia Tech, Blacksburg, VA 24061, USA*

⁹ *Dipartimento di Fisica e Astronomia, Università di Padova, vicolo Osservatorio, 3, I-35122 Padova, Italy*

¹⁰ *INAF – Osservatorio Astronomico di Trieste, via Tiepolo 11, I-34131 Trieste, Italy*

¹¹ *Department of Physics and Astronomy, University of British Columbia, 6224 Agricultural Road, Vancouver, BC V6T 1Z1, Canada*

¹² *California Institute of Technology, 1200 E. California Blvd., Pasadena, CA 91125, USA*

Submitted 23 January 2014. Accepted 31 March 2014.

ABSTRACT

We have investigated the gas content of a sample of several hundred AGN host galaxies at $z < 1$ and compared it with a sample of inactive galaxies, matched in bins of stellar mass and redshift. Gas masses have been inferred from the dust masses, obtained by stacked Herschel far-IR and sub-mm data in the GOODS and COSMOS fields, under reasonable assumptions and metallicity scaling relations for the dust-to-gas ratio. We find that AGNs are on average hosted in galaxies much more gas rich than inactive galaxies. In the vast majority of stellar mass bins, the average gas content of AGN hosts is higher than in inactive galaxies. The difference is up to a factor of ten higher in low stellar mass galaxies, with a significance of 6.5σ . In almost half of the AGN sample the gas content is three times higher than in the control sample of inactive galaxies. Our result strongly suggests that the probability of having an AGN activated is simply driven by the amount of gas in the host galaxy; this can be explained in simple terms of statistical probability of having a gas cloud falling into the gravitational potential of the black hole. The increased probability of an AGN being hosted by a star-forming galaxy, identified by previous works, may be a consequence of the relationship between gas content and AGN activity, found in this paper, combined with the Schmidt-Kennicutt law for star formation.

Key words: methods: data analysis – galaxies: active – galaxies: ISM

1 INTRODUCTION

During the past decades several studies have revealed a connection between the mass of Black Holes hosted in galactic nuclei and the properties of their host galaxies

(e.g. Magorrian et al. 1998; Ferrarese & Merritt 2000; Marconi & Hunt 2003). Moreover, the redshift evolution of the cosmic Star Formation Rate (SFR) and SMBH accretion rate density are very similar (Boyle & Terlevich 1998; Granato et al. 2001; Marconi et al. 2004; Hopkins & Beacom 2006; Silverman et al. 2009; Aird et al. 2010). This “co-evolution” has led various authors to investigate a possible connection between the presence of Active Galactic Nuclei (AGN, which traces the SMBH growth) and the star formation properties of galaxies. A

^{*} *Herschel* is an ESA space observatory with science instruments provided by European-led Principal Investigator consortia and with important participation from NASA.

[†] E-mail: fabio.vito@unibo.it

correlation was indeed observed between star formation and nuclear activity in numerous works at high AGN luminosities (e.g. Lutz et al. 2008, 2010; Shao et al. 2010; Rosario et al. 2012), while at low AGN luminosities this link is more debated, with Silverman et al. (2009) reporting no significant difference in the SFR between active and inactive galaxies, while Santini et al. (2012) found a slight enhancement for AGN-hosting galaxies. They also reported that the enhancement of star formation activity in AGN with respect to the bulk of inactive galaxies disappeared if quiescent galaxies were discarded, i.e. AGN are more likely hosted in star forming galaxies.

The gas content is often regarded as a more fundamental property of galaxies, with respect to the SFR. The SFR is tightly related to the gas content through the Schmidt-Kennicutt relation (Schmidt 1959; Kennicutt 1998, SK relation hereafter). Currently, one of the most favored scenarios is that the cosmic evolution of the star formation rate in galaxies is mostly a consequence, through the SK relation, of the more fundamental evolution of their (molecular) gas content (e.g. Obreschkow & Rawlings 2009; Lagos et al. 2011).

Within the context of AGNs, gas is the fundamental ingredient both for nuclear activity and star formation. Possible differences in terms of star formation properties between AGNs hosts and inactive galaxies could be due to more fundamental differences in terms of gas content, as recently argued by Santini et al. (2012) and Rosario et al. (2012, 2013). Therefore, it is most important to obtain information on the gas content of AGN host galaxies, possibly as a function of galaxy properties (e.g. stellar mass) and redshift.

The molecular gas content can be inferred from the luminosity of the CO millimeter transitions, by assuming a proper CO-to-H₂ conversion factor. However, CO observations are very time consuming, and surveys of large samples are extremely difficult and time demanding. Alternatively, the total (molecular and atomic) gas mass can be derived from the dust content, inferred from the FIR-submm SED, by assuming a dust-to-gas ratio (DGR; e.g. Eales et al. 2010; Leroy et al. 2011; Magdis et al. 2011). The uncertainties on the dust-to-gas ratio and its dependence on metallicity are similar to those affecting the CO-to-H₂ conversion factor, making the two methods comparable in terms of accuracy, at least at metallicities $12+\log(\text{O}/\text{H}) > 8.0$ (Bolatto et al. 2013; Rémy-Ruyer et al. 2013).

In this work we exploit the dust method for measuring the gas masses in AGN host galaxies. In particular, gas masses are obtained from the dust mass derived from the FIR SED of several hundred AGN host galaxies at $z < 1$, along with a control sample of normal galaxies selected in the same stellar mass and redshift ranges. The aim of this work is to investigate differences in terms of gas content between AGN hosts and the bulk of the galaxy population (i.e. star forming and quiescent galaxies), in bins of stellar mass and redshift, to avoid potential biases caused by the dependency of the gas content on these two quantities. We make use of a stacking procedure to increase the luminosity completeness of the studied samples (§ 3.2).

2 DATA SET AND SAMPLE SELECTION

We selected a sample of AGN at $z \leq 1$ (as well as normal galaxies for the control sample) in the COSMOS, GOODS-S and GOODS-N fields. The choice of these fields was driven by the wide multiwavelength coverage provided by a number of surveys, which is crucial to derive reliable properties (redshift, stellar mass, star-formation rate and dust mass).

We used the Far-Infrared (FIR) data from the PACS Evolutionary Probe (PEP, Lutz et al. 2011) and the Herschel Multi-tiered Extra-galactic Survey (HerMES, Oliver et al. 2012) programs, which cover the three fields used in this work. The former was performed with the PACS camera (70, 100 and 160 μm ; Poglitsch et al. 2010) while the latter with the SPIRE camera (250, 350 and 500 μm ; Griffin et al. 2010), both on board of the Herschel Space Observatory (Pilbratt et al. 2010). Herschel catalogues are based on prior information on MIPS 24 μm positions and fluxes. The PEP catalogue was described by Lutz et al. (2011) and Berta et al. (2011), while the HerMES catalogue was presented by Roseboom et al. (2010, 2012). Since only the GOODS-S field was observed at 70 μm , following Santini et al. (2013, S13 hereafter), who reported that the exclusion of that band does not significantly affect the results, we will not use the 70 μm data, to use a consistent procedure among all the fields.

For the GOODS-S field we used the optical/near-IR photometric data from the GOODS-MUSIC catalogue (Grazian et al. 2006; Santini et al. 2009) and the X-ray counterpart information from the 4 Ms *Chandra* Deep Field South (CDF-S) main catalogue (Xue et al. 2011). In the GOODS-N field we collected the multiwavelength data from the PEP team catalogue (Berta et al. 2011) and the X-ray data from the 2 Ms *Chandra* Deep Field North catalogue (Alexander et al. 2003; Bauer et al. 2004). Finally, in the COSMOS field we used the Ilbert et al. (2009) and McCracken et al. (2010) multiwavelength catalogues and the *Chandra* (Civano et al. 2012) and XMM (Brusa et al. 2010) COSMOS optical identification catalogues, complemented by the photometric redshifts presented by Salvato et al. (2011). All the catalogues are supplemented with spectroscopic or photometric redshifts. Photometric redshift for inactive galaxies in COSMOS and GOODS-N lacking redshift information in the above-mentioned catalogues were computed by using the EAZY code (Brammer et al. 2008).

We applied two selection criteria to the parent sample in the three fields: 1) signal-to-noise ratio (SNR) ≥ 10 in the K-band; 2) $z \leq 1$. The K-band selection ensures that we can derive reliable estimates for the stellar mass (following S13), while the redshift cut ensures that the Herschel bands are not probing rest-frame wavelengths that may be significantly affected by AGN heating and reprocessing (which may affect our estimation of the dust masses). Indeed, Rosario et al. (2012) have shown that out to $z \sim 1$ the PACS colors are consistent with those typical of star forming galaxies, while some AGN contamination to the 100 μm may occur at higher redshift.

Once these selections are applied, we divided the resulting objects into AGN and a galaxy samples. In COSMOS, we considered an X-ray detected object to be an AGN following its optical classification (Brusa et al. 2010; Civano et al.

2012) or best-fitting SED template (Salvato et al. 2011) or if its absorption-corrected luminosity in the rest-frame 2 – 10 keV band, where available, is $L_X \geq 10^{42} \text{erg s}^{-1}$. This threshold is a compromise between the sample size and the contamination by purely powerful star-forming galaxies (Ranalli et al. 2003). The luminosities were collected from Lanzuisi et al. (2013) and Mainieri et al. (2007, 2011), who performed a spectral analysis on a sample of bright sources in the *Chandra*-COSMOS (Elvis et al. 2009) and XMM-COSMOS (Cappelluti et al. 2009) catalogues, respectively. Intrinsic luminosities of all the XMM-COSMOS selected sources were also derived by the XMM-COSMOS team using the observed fluxes and Hardness Ratio HR (see Merloni et al. 2013). In GOODS-S we assumed the Xue et al. (2011) classification and luminosity for the X-ray sources. In GOODS-N we used the X-ray detected AGN sample of Bauer et al. (2004). The luminosities of the X-ray selected AGN for which this information could be retrieved are in the range $10^{41} \lesssim L_X < 10^{45} \text{erg s}^{-1}$, and only ~ 5 per cent of them have $L_X > 10^{44} \text{erg s}^{-1}$. Given the limiting fluxes of the X-ray samples, the most obscured AGN can still remain undetected. In order to at least partially recover them, we applied the IRAC power-law selection by Donley et al. (2012). The resulting AGN sample consists in 801 objects, of which 631 X-ray selected (in any X-ray band considered in the above-mentioned catalogues; 486 in COSMOS and 145 in GOODS-S+N) and 255 IRAC selected (241 in COSMOS and 14 in GOODS-S+N). Eighty-five AGN (78 in COSMOS and 7 in GOODS-S+N) are in common between the two selections. All the sources which do not satisfy any of the AGN selection criterion in each field are automatically classified as inactive galaxies (~ 175000 objects).

3 PARAMETERS DERIVATION

In this section we describe how the physical parameters for our sample of AGN and galaxies were derived. In order to avoid selection effects due to redshift, stellar mass and luminosity affecting the dust mass (and hence the gas mass) measurement and distribution, we adopted a stacking technique to derive the average FIR fluxes in bins of stellar mass and redshift. This method ensures a high level of completeness, since only a small fraction of sources are individually detected by Herschel, especially in the longest wavelength bands.

3.1 Stellar Mass

Stellar masses for AGN-hosting galaxies in the sample were derived using the same method as in Santini et al. (2012), where several consistency tests were also performed. The observed optical photometry was fitted with a combined library of stellar synthetic templates (Bruzual & Charlot 2003) and pure AGN emission templates affected by levels of absorption (Silva et al. 2004) associated with different column densities N_H .

In order to break the degeneracies between the different fit parameters, the AGN were classified into Type I (unabsorbed) and Type II (absorbed) sources on the basis of optical spectroscopic classification (where available), best-fitting Spectral Energy Distribution (SED) template from

Salvato et al. (2011) and intrinsic absorption derived from X-ray data analysis (Lanzuisi et al. 2013; Mainieri et al. 2007, 2011; Bauer et al. 2004). Sources for which all these priors are lacking, as well as X-ray undetected AGN (i.e. Spitzer selected AGN) were considered as Compton-Thin Type II AGN. Moreover, by averaging the two templates of moderate absorption, the four Silva et al. (2004) templates were reduced to three: unabsorbed ($N_H < 10^{22} \text{cm}^{-2}$), Compton-Thin absorbed ($10^{22} < N_H < 10^{24} \text{cm}^{-2}$) and Compton-Thick absorbed ($N_H > 10^{24} \text{cm}^{-2}$). Only the most suitable template, based on the above classification, was fitted to each AGN. In particular, the unabsorbed, absorbed Compton Thin and absorbed Compton Thick templates were used for 100, 694 and 7 sources, respectively.

The fit was performed through a χ^2 minimization up to $5 \mu\text{m}$ rest-frame, since the Bruzual & Charlot (2003) templates do not include emission from dust reprocessing, assuming an exponentially declining star-formation history and a Salpeter IMF for the stellar component. Each flux was weighted by the inverse of the photometric error and the redshift of each object was fixed during the fit. The stellar mass was derived by the best-fitting stellar component alone.

3.2 Stacking procedure

AGN and galaxies are divided into 6 stellar mass bins (from $\log(M_*/M_\odot) = 9$ to 12) and 4 redshift bins. The number of AGN and galaxies in each bin is reported in Table 1. Hereafter, the stellar mass corresponding to each bin is assumed to be the mean stellar mass of the objects in the bin, with uncertainty equal to one standard deviation (typically ~ 0.14 dex for both AGN and galaxies). We adopt the stacking procedure implemented by S13, where details on the stacking procedure are given (see also Shao et al. 2010, Rosario et al. 2012 and Santini et al. 2012). However, in contrast with Santini et al., we do not bin in Star Formation Rate (SFR), since our goal is to investigate if differences in terms of gas content between AGNs and normal galaxies may actually be at the origin of their claimed SFR differences, hence we do not want to include any *a priori* selection or binning on the SFR.

Details on the stacking procedure are given in S13 (2013). Here we only briefly summarize the basic steps. For each Herschel band we excluded areas on the map where the integration time is lower than half the maximum, to avoid regions of high noise level. Then, for each $z - M_*$ bin containing at least 10 objects, we stack on the residual image (in which all the 3σ detected objects were subtracted) of each Herschel band at the position of the undetected sources in the bin, weighting with the inverse of the square of the error map. Fluxes on the stacked images were measured through a PSF fitting (for the PACS bands) or from the value of the central pixel (on the SPIRE images). Errors on the stacked fluxes were computed through a bootstrap procedure. Finally, the average flux S in each Herschel band is computed as:

$$S = \frac{S_{stack} \times N_{stack} + \sum_{i=1}^{N_{det}} S_i}{N_{stack} + N_{det}} \quad (1)$$

where S_{stack} is the stacked flux of the N_{stack} undetected

Table 1. Number of AGN and galaxies (between brackets) stacked in each $z - M_*$ bin (see § 3.2). The bins that fulfil the conditions in § 3.3 are in boldface.

z	$\log(M_*/M_\odot)$					
	9-10	10-10.5	10.5-11	11-11.25	11.25-11.5	11.5-12
0.0-0.3	10 (3120)	< 10 (735)	17 (496)	< 10 (125)	< 10 (37)	< 10 (< 10)
0.3-0.6	48 (13800)	32(3881)	65 (2795)	42 (801)	22 (414)	16 (117)
0.6-0.8	29 (10621)	24 (5065)	61 (3071)	43 (1018)	42 (504)	16 (199)
0.8-1.0	17 (6767)	19 (6209)	72 (4393)	70 (1372)	53 (754)	30 (295)

objects in the bin and S_i is the flux of each of the N_{det} detected objects at the 3σ confidence level.

3.3 Dust Mass

FIR emission in star forming galaxies is mainly due to galactic cold dust, heated by young stars. The dust mass can be inferred by fitting dust emission models to the FIR fluxes varying the temperature distribution and normalization of the far-IR SED. We considered only $z - M_*$ bins in which the stacked flux has a 3σ significance in at least three Herschel bands, at least one of which between the 350 and 500 μm bands. This requirement ensures a good sampling of the dust emission peak and, hence, reliable estimates of the dust mass.

We performed a χ^2 minimization to the analytical SED templates by Draine & Li (2007) (which span a broad range of dust temperature distributions) and, in each $z - M_*$ bin, the best-fitting dust mass (M_d) was derived from the normalization of the template corresponding to the minimum χ^2 . Further details on the method are given in S13. Errors were estimated from the range of M_d covered by all the templates within $\Delta\chi^2 = 1$ from the value of the best fitting template. Regarding the AGN sample, since emission from AGN-heated dust could contribute to the FIR fluxes, especially in the PACS bands, we added the Silva et al. (2004) AGN SEDs during the Draine & Li (2007) templates fit, leaving their normalization free to vary. However, we shall mention that the results on the dust masses are essentially unchanged even by neglecting the AGN contribution in the SED fitting; this is not surprising, not only because AGN heating contribute mostly at mid-IR wavelengths (which are not relevant for the dust mass derivation), but also because most of the AGNs in our sample do not have extreme luminosities (see § 2).

3.4 Gas mass

The total gas mass (M_{gas} , which incorporates both the molecular and atomic phases) can be inferred from the dust mass through a dust-to-gas ratio (DGR; e.g. Eales et al. 2010; Magdis et al. 2012): $M_{gas} = M_d/\text{DGR}$. In order to derive the DGR, we assumed that a fixed fraction of metals is incorporated into dust grains (e.g. Draine et al. 2007 and references therein; Leroy et al. 2011; Smith et al. 2012; Corbelli et al. 2012; Sandstrom et al. 2012) and that the DGR scales linearly with the gas metallicity, traced by the oxygen abundance (Draine et al. 2007):

$$\text{DGR} = 0.01 \cdot 10^{Z-Z_\odot}. \quad (2)$$

This assumption is observationally found to be a good approximation down to metallicities $Z=12+\log(\text{O}/\text{H})\sim 8.0$ (Rémy-Ruyer et al. 2013), which is certainly lower than the metallicity range spanned by our sample. We refer to S13 for a more extended discussion on this method to derive the gas mass from the dust mass.

We derived the mean gas metallicity (Z) in each $z - M_*$ bin from the Fundamental Metallicity Relation (FMR) by Mannucci et al. (2010, 2011), who found a narrow (scatter of ~ 0.05 dex) relation between M_* , SFR and Z in local and high-redshift galaxies.

The average SFR for each $z - M_*$ bin was computed from the total 8–1000 μm luminosity (L_{IR}), derived by integration of the best-fitting dust emission template used in § 3.3:

$$\text{SFR}[M_\odot/\text{yr}] = 1.8 \times 10^{-10} L_{IR}[L_\odot]. \quad (3)$$

Stellar mass and SFR were converted from a Salpeter to a Chabrier IMF (Davé 2008; Santini et al. 2012), as Mannucci et al. (2010, 2011) assumed. Errors on Z were estimated considering the FMR intrinsic scatter and the errors on M_* . Errors on SFR were ignored, since they are negligible with respect to the other uncertainties (typically $\Delta\log\text{SFR}/\log\text{SFR} \simeq 0.04$). Finally, errors on M_d and Z were propagated to derive the uncertainties on M_{gas} . We shall mention that if the FMR is ignored and the metallicities are simply inferred from the mass-metallicity relation (Tremonti et al. 2004) and assuming a redshift evolution of this relation (Maiolino et al. 2008; Troncoso et al. 2013), the results remain unchanged. More generally the bulk of the M_{gas} variations are due to the variations of M_{dust} , while variations and uncertainties in the DGR play a secondary role (i.e. the main results do not change even if we only consider the dust mass instead of the gas mass, as we will discuss later on).

We also note that the effect of the presence of an AGN on the DGR, if any, would be to decrease its value with respect to inactive galaxies. Indeed, the hard nuclear radiation is expected to make the environment less favourable to dust survival. Nonetheless, we assumed the same DGR for AGN hosts as for inactive galaxies. As our results will show, this turns out to be a conservative approach.

4 RESULTS AND DISCUSSION

Fig. 1 (left panel) shows the average gas mass as a function of the stellar mass of the AGN and galaxy samples for each $z - M_*$ bin which fulfils the requirements described in § 3.3. The gas mass of galaxies increases with stellar mass, while the

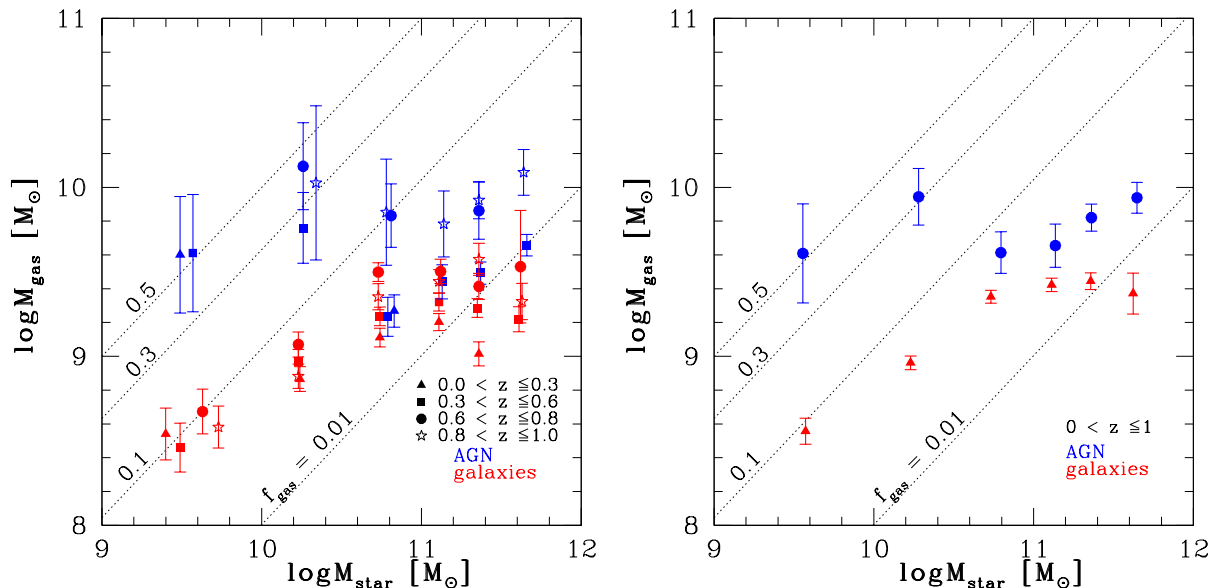


Figure 1. Gas mass as a function of the stellar mass for the AGN (blue symbols) and normal galaxy (red symbols) samples, in different redshift bins (identified by different symbols; left panel) and averaged over the redshift bins (right panel). Loci of constant gas fraction, for different values, are shown with dotted lines.

gas fraction, defined as $f_{\text{gas}} = M_{\text{gas}} / (M_{\text{gas}} + M_{\star})$, increases towards lower stellar masses, as already reported by S13.

The most interesting result is that the AGN hosts gas masses are systematically higher than in the galaxy sample, in nearly all bins of stellar mass and redshift. Since this result does not show any evident dependence on redshift, in Fig. 1 (right panel) we show the gas mass in the different stellar mass bins, averaged over the redshift bins using weights corresponding to the number of objects in each bin. Largely consistent results are found by computing the unweighted averages. The same qualitative relations hold if one considers the directly-measured dust mass instead of the more physically relevant gas mass. Indeed, as also reported in § 3.4, gas mass derivation is strongly dominated by the dust mass, with variations on the DGR being second order effects.

Fig. 2 shows the distribution of $M_{\text{gas,AGN}}/M_{\text{gas,gal}}$, for all redshift and stellar mass bins for which this comparison can be made. Clearly, in nearly all bins (more specifically, in 94% of them), $M_{\text{gas,AGN}}/M_{\text{gas,gal}} > 1$. In 44% of the bins the gas mass in AGN hosts is higher by more than a factor of three with respect to normal galaxies. The same result is shown in Fig. 3 in terms of gas fractions, $f_{\text{gas,AGN}}/f_{\text{gas,gal}}$.

To better quantify the significance of the result, Table 2 gives the mean $M_{\text{gas,AGN}}/M_{\text{gas,gal}}$ ratio, obtained by averaging the results in three different stellar mass ranges. The strongest difference is clearly at $\log(M_{\text{star}}/M_{\odot}) < 10.5$, where the gas mass of AGN hosts is on average an order of magnitude higher than in normal galaxies, with a significance of 6.5σ . However, the difference between AGN and normal galaxies in terms of gas masses is significant at $\sim 3 - 7\sigma$ also at $\log(M_{\text{star}}/M_{\text{odot}}) > 10.5$.

We checked that no significant change in the results are obtained considering different mass or redshift bins. The low stellar-mass bins can be affected by incompleteness, also because the K-band selection preferentially rejects low mass

Table 2. Mean $\log(M_{\text{gas,AGN}}/M_{\text{gas,gal}})$ (computed in $z - M_{\star}$ bins) for three different mass ranges.

$\log(\frac{M_{\star}}{M_{\odot}})$	9-10.5	10.5-11.25	11.25-12
$\langle \log(\frac{M_{\text{gas,AGN}}}{M_{\text{gas,gal}}}) \rangle$	1.04 ± 0.16	0.24 ± 0.08	0.44 ± 0.06

objects. However, the same level of completeness is expected to characterize the AGN and galaxy samples, as the K-band is dominated by the stellar component. The main conclusion holds, besides the loss of statistics, even repeating the analysis separately on X-ray detected and undetected AGN, as well as applying different cuts in L_X .

Since gas accretion onto Super Massive Black Holes (SMBH) is the process at the origin of nuclear activity, whatever the mechanisms that drives the gas into the central regions are, it is not surprising that AGNs are preferentially hosted by gas rich galaxies (see also Silverman et al. 2009). Indeed, the conditions for gas accretion are statistically easier to be fulfilled in presence of a larger gas content. Beyond these simple statistical arguments, models have been proposed that ascribe AGN secular fuelling to disk instabilities (Bournaud et al. 2011), which are stronger in gas rich disks. Our results support this scenario.

As discussed above, the gas content is also the fundamental ingredient driving star formation in galaxies, through the SK relation. Several works have found a relation between strong nuclear activity and enhanced SFR with respect to inactive galaxies (e.g Lutz et al. 2008, 2010; Shao et al. 2010; Rosario et al. 2012). Rosario et al. (2013) and Santini et al. (2012) found that the Herschel detection fraction for AGN is higher than for galaxies and concluded that AGN are more likely to be hosted by star forming galaxies.

Given the dependency of the SFR on the gas content

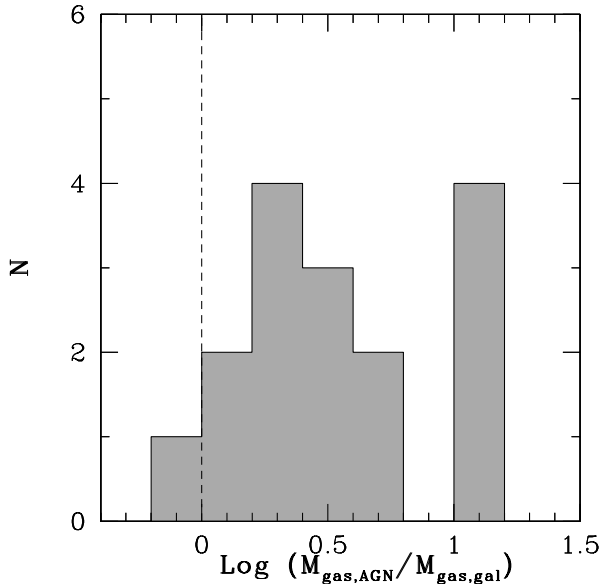


Figure 2. Distribution of the ratio between the gas mass in AGN hosts and in normal galaxies, inferred within the same $z - M_*$ bins.

and the result obtained by us, the enhanced star formation in AGN galaxies appears to be primarily the result of a larger (on average) gas content, with respect to the bulk of the galaxy population (star forming and quiescent) at similar stellar masses, as already suggested by Rosario et al. (2012, 2013) and Santini et al. (2012). However, the differences in terms of SFR are less clear with respect to the differences found by us in terms of gas content, probably because of the additional spread introduced by the SK relation, and the contribution of triggering mechanisms (e.g. galaxy interactions), which may affect the star formation efficiency per unit gas mass. It is beyond the scope of this paper to further discuss the level and nature of enhanced SFR in AGN hosts.

The main important result of our work is that AGN host galaxies are characterized by much larger amounts of gas, strongly suggesting that generally AGN activity in galaxies is simply fostered by a larger content of gas, without invoking specific triggering mechanisms.

5 CONCLUSIONS

Making use of the wide multiwavelength data available in the COSMOS, GOODS-S and GOODS-N fields, we selected a sample of AGN and galaxies at $z < 1$. A stacking procedure on the Herschel maps was implemented to derive the average Herschel fluxes in bins of stellar mass and redshift. The stacked FIR fluxes were then used to derive the average dust mass and, under reasonable assumptions, the average gas mass of AGN hosts and normal galaxies. Finally we compared the average gas mass of AGN hosts and inactive galaxies in the same $z - M_*$ bins.

We find that, at a given stellar mass and redshift, AGNs are hosted in galaxies much more gas-rich than inactive ones. The difference is strongest at low stellar masses, $\log(M_*/M_\odot) < 10.5$, where the gas mass in AGN hosts

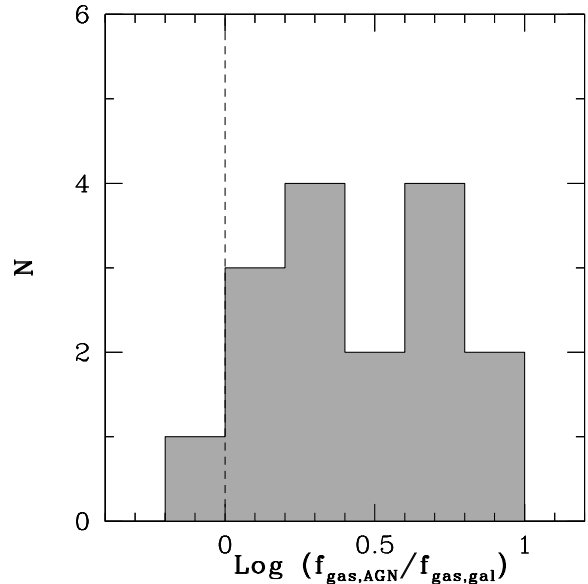


Figure 3. Distribution of the ratio between the gas fraction in AGN hosts and in normal galaxies, inferred within the same $z - M_*$ bins.

is on average ten times higher than in normal galaxies (a result significant at 6.5σ). Significantly higher gas masses, relative to the normal galaxy population, are however also observed in AGN hosts with stellar masses higher than $\log(M_*/M_\odot) > 10.5$. Taken altogether, in nearly all stellar mass and redshift bins AGN host galaxies have higher gas content than normal galaxies; in almost half of the sample the gas fraction of AGN host galaxies is more than three times higher than in normal galaxies.

Our result strongly suggests that the likelihood of having an AGN in a galaxy is primarily given by the amount of gas in the host galaxy, while dynamical triggering processes (bars, galaxy mergers and interactions) likely play a secondary role, at least in the luminosity range probed by us. This result can be interpreted in simple statistics terms that it is more likely that a gas cloud falls into the potential of the supermassive black hole if there are overall more gas clouds in the host galaxy. More elaborated models, in which secular fuelling of AGNs is caused by disk instabilities, which are stronger in more gas rich disks, are also supported by our results.

ACKNOWLEDGMENTS

We acknowledge support from the Italian Space Agency under the ASI-INAF contract I/009/10/0 and from INAF under the contract PRIN-INAF-2012. FV thanks B. Luo for kindly providing Chandra ID's of MUSIC counterparts in GOODS-S and I. Delvecchio for useful discussion on SED fitting procedure. This paper uses data from *Herschel*'s photometers PACS and SPIRE. PACS has been developed by a consortium of institutes led by MPE (Germany) and including UVIE (Austria); KU Leuven, CSL, IMEC (Belgium); CEA, LAM (France); MPIA (Germany); INAF-IFSI/OAA/OAP/OAT, LENS, SISSA (Italy); IAC

(Spain). This development has been supported by the funding agencies BMVIT (Austria), ESA-PRODEX (Belgium), CEA/CNES (France), DLR (Germany), ASI/INAF (Italy), and CICYT/MCYT (Spain). SPIRE has been developed by a consortium of institutes led by Cardiff University (UK) and including Univ. Lethbridge (Canada); NAOAC (China); CEA, LAM (France); IFSI, Univ. Padua (Italy); IAC (Spain); Stockholm Observatory (Sweden); Imperial College London, RAL, UCL-MSSL, UKATC, Univ. Sussex (UK); and Caltech, JPL, NHSC, Univ. Colorado (USA). This development has been supported by national funding agencies: CSA (Canada); NAOAC (China); CEA, CNES, CNRS (France); ASI (Italy); MCINN (Spain); SNSB (Sweden); STFC, UKSA (UK); and NASA (USA).

REFERENCES

- Aird J. et al., 2010, *MNRAS*, 401, 2531
 Alexander D. M. et al., 2003, *AJ*, 126, 539
 Bauer F. E., Alexander D. M., Brandt W. N., Schneider D. P., Treister E., Hornschemeier A. E., Garmire G. P., 2004, *AJ*, 128, 2048
 Berta S. et al., 2011, *A&A*, 532, A49
 Béthermin M., Dole H., Beelen A., Aussel H., 2010, *A&A*, 512, A78
 Bolatto A. D., Wolfire M., Leroy A. K., 2013, *ARA&A*, 51, 207
 Bongiorno A. et al., 2007, *A&A*, 472, 443
 Bournaud F., Dekel A., Teyssier R., Cacciato M., Daddi E., Juneau S., Shankar F., 2011, *ApJ*, 741, L33
 Boyle B. J., Terlevich R. J., 1998, *MNRAS*, 293, L49
 Brammer G. B., van Dokkum P. G., Coppi P., 2008, *ApJ*, 686, 1503
 Brusa M. et al., 2010, *ApJ*, 716, 348
 Bruzual G., Charlot S., 2003, *MNRAS*, 344, 1000
 Calzetti D., Armus L., Bohlin R. C., Kinney A. L., Koornneef J., Storchi-Bergmann T., 2000, *ApJ*, 533, 682
 Cappelluti N. et al., 2009, *A&A*, 497, 635
 Civano F. et al., 2011, *ApJ*, 741, 91
 Corbelli E. et al., 2012, *A&A*, 542, A32
 Daddi E. et al., 2010, *ApJ*, 714, L118
 Davé R., 2008, *MNRAS*, 385, 147
 Donley J. L. et al., 2012, *ApJ*, 748, 142
 Draine B. T., Li A., 2007, *ApJ*, 657, 810
 Draine B. T. et al., 2007, *ApJ*, 663, 866
 Eales S. A. et al., 2010, *A&A*, 518, L62
 Elvis M. et al., 2009, *ApJS*, 184, 158
 Ferrarese L., Merritt D., 2000, *ApJ*, 539, L9
 Fiore F. et al., 2003, *A&A*, 409, 79
 Fontanot F., De Lucia G., Monaco P., Somerville R. S., Santini P., 2009, *MNRAS*, 397, 1776
 Genzel R. et al., 2010, *MNRAS*, 407, 2091
 Granato G. L., Silva L., Monaco P., Panuzzo P., Salucci P., De Zotti G., Danese L., 2001, *MNRAS*, 324, 757
 Grazian A. et al., 2006, *A&A*, 449, 951
 Griffin M. J. et al., 2010, *A&A*, 518, L3
 Hasinger G., Miyaji T., Schmidt M. 2005, *A&A*, 441, 417
 Hopkins A. M., Beacom J. F. 2006, *ApJ*, 651, 142
 Kennicutt R. C., 1998, *ApJ*, 498, 541
 Ilbert O. et al., 2009, *ApJ*, 690, 1236
 La Franca F. et al., 2005, *ApJ*, 635, 864
 Lagos C. D. P., Baugh C. M., Lacey C. G., Benson A. J., Kim H.-S., Power C., 2011, *MNRAS*, 418, 1649
 Lanzuisi G. et al., 2013, *MNRAS*, 431, 978
 Leroy A. K. et al., 2011, *ApJ*, 737, 12
 Lutz D. et al., 2008, *ApJ*, 684, 853
 Lutz D. et al., 2010, *ApJ*, 712, 1287
 Lutz D. et al., 2011, *A&A*, 532, A90
 Magdis G. E. et al., 2011, *ApJ*, 740, L15
 Magdis G. E. et al., 2012, *ApJ*, 760, 6
 Magorrian J. et al., 1998, *AJ*, 115, 2285
 Mainieri V. et al., 2007, *ApJS*, 172, 368
 Mainieri V. et al., 2011, *A&A*, 535, A80
 Maiolino R. et al., 2008, *A&A*, 488, 463
 Mannucci F., Cresci G., Maiolino R., Marconi A., Gnerucci A., 2010, *MNRAS*, 408, 2115
 Mannucci F., Salvaterra R., Campisi M. A., 2011, *MNRAS*, 414, 1263
 Marconi A., Hunt L. K., 2003, *ApJ*, 589, L21
 Marconi A., Risaliti G., Gilli R., Hunt L. K., Maiolino R., Salvati M., 2004, *MNRAS*, 351, 169
 McCracken H. J., et al., 2010, *ApJ*, 708, 202
 Merloni A. et al., 2014, *MNRAS*, 437, 3550
 Obreschkow D., Rawlings S., 2009, *ApJ*, 696, L129
 Oliver S. J. et al., 2012, *MNRAS*, 424, 1614
 Pilbratt G. L. et al., 2010, *A&A*, 518, L1
 Poglitsch A. et al., 2010, *A&A*, 518, L2
 Ranalli P., Comastri A., Setti G., 2003, *A&A*, 399, 39
 Rémy-Ruyer A. et al., 2013, *arXiv*, arXiv:1312.3442
 Rosario D. J. et al., 2012, *A&A*, 545, A45
 Rosario D. J. et al., 2013, *ApJ*, 771, 63
 Roseboom I. G. et al., 2010, *MNRAS*, 409, 48
 Roseboom I. G., et al., 2012, *MNRAS*, 419, 2758
 Salvato M. et al., 2011, *ApJ*, 742, 61
 Sandstrom K. M. et al., 2012, *ApJ*, 744, 20
 Santini P. et al., 2009, *A&A*, 504, 751
 Santini P. et al., 2012, *A&A*, 538, A33
 Santini, P. et al., 2012, *A&A*, 540, A109
 Santini P. et al., 2013, *arXiv*:1311.3670
 Schmidt M., 1959, *ApJ*, 129, 243
 Scoville N. et al., 2014, *arXiv*, arXiv:1401.2987
 Shao L. et al., 2010, *A&A*, 518, L26
 Silva L., Maiolino R., Granato, G. L., 2004, *MNRAS*, 355, 973
 Silverman J. D. et al., 2009, *ApJ*, 696, 396
 Smith D. J. B. et al., 2012, *MNRAS*, 427, 703
 Tacconi L. J. et al., 2013, *ApJ*, 768, 74
 Tremonti C. A. et al., 2004, *ApJ*, 613, 898
 Troncoso P. et al., 2013, *arXiv*, arXiv:1311.4576
 Xue Y. Q. et al., 2011, *ApJS*, 195, 10

This paper has been typeset from a $\text{\TeX}/\text{\LaTeX}$ file prepared by the author.